Dips and Rims in Dried Colloidal Films

C. Parneix,[1] P. Vandoolaeghe,[1] V. S. Nikolayev,[1,2] D. Quéré,[1] J. Li,[1] and B. Cabane[1]
[1]PMMH-ESPCI-P6-P7, CNRS UMR 7636, 10, rue Vauquelin, 75231 Paris Cedex 5, France
[2]Service des Basses Températures, INAC/CEA-Grenoble, France
(Received 2 February 2010; published 29 December 2010)

We describe a spatial pattern arising from the nonuniform evaporation of a colloidal film. Immediately after the film deposition, an obstacle is positioned above its free surface, minimizing evaporation at this location. In a first stage, the film dries everywhere but under the obstacle, where a liquid region remains. Subsequently, this liquid region evaporates near its boundaries with the dry film. This loss of water causes a flow of liquid and particles from the center of the obstructed region to its periphery. The final film has a dip surrounded by a rim whose diameter is set by the obstacle. This turns out to be a simple technique for structuring films of nanometric thickness.

DOI: 10.1103/PhysRevLett.105.266103 PACS numbers: 68.03.Fg, 47.54.−r, 47.55.np, 47.57.J−

Evaporation from a liquid is rarely uniform. The flux of evaporating molecules may vary owing to convection currents in the gaseous environment above the surface or to a nonuniform temperature in the liquid. Geometrical effects can also play a role, especially in films with pinned contact lines [1,2]. Enhanced evaporation near the edges of the film and surface tension forces combine to produce a fluid flow from the center of the film to its periphery, which leads to the formation of rings of deposited colloidal particles after evaporation[3–6]. In films of concentrated colloidal dispersions, a drying front sweeps across the film, at a speed determined by the joint effects of evaporation and fluid flow [7,8].

Another remarkable situation applies to the flow in a film covered by a ''mask'' that limits evaporation [7,9,10]. Indeed, when the mask with holes is positioned at a short distance above the liquid surface, evaporation primarily occurs under the holes so that surface tension drives a flow of liquid to replace this loss. If the liquid contains dispersed colloidal particles, the solid film after evaporation is a set of hills that match the hole locations. This technique for modulating the thickness of a dried colloidal film has been called ''evaporative lithography.''

Here we report observations also arising from nonuniform evaporation, caused by a different set of transport phenomena. This phenomenon takes place in very thin (micrometric) films of colloidal dispersions. Evaporation from the film surface is free everywhere but in one location, where a solid disk placed above the surface limits evaporation [Fig. 1(a)]. This device produces dried films that have a marked dip surrounded by a thick rim at the place below the obstacle [Fig. 1(b)]. The dip is significantly thinner than the rest of the dried film [Fig. 2(a)], and it can nearly reach the substrate surface, depending on the distance between the disk and the film. In addition, the dip size is found to match the obstacle size [Fig. 2(b)], which yields a precise control for the final pattern of the dried film. For a film thickness in the range of visible light wavelengths, dips are visible with a naked eye, so that the appearance of the substrate can be conveniently modulated using this technique of differential evaporation.

Figure 1(a) presents the geometry of our experiment. The substrate is a glass slide with a surface made hydrophilic by abrasion with a fine ceria powder. The liquid film

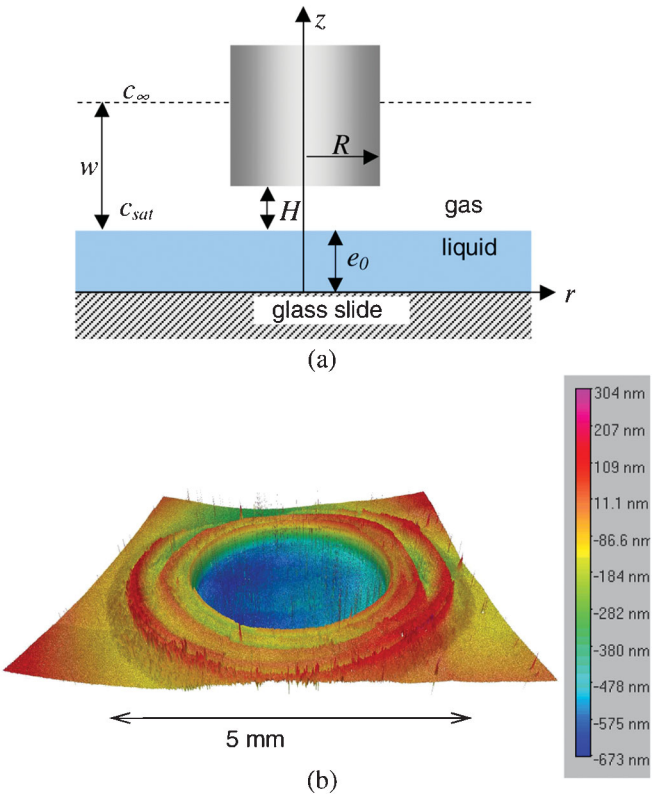

FIG. 1 (color). (a) Setup for controlling the film evaporation. The film is shown in its initial state. (b) A dip surrounded by a rim forms below the obstacle. Profile of the dried film obtained for $e_0 = 3.5\ \mu$m, $2R = 5$ mm, and $H = 1$ mm observed with an optical profilometer (zero of the vertical axis corresponds to the film level far from the obstacle).

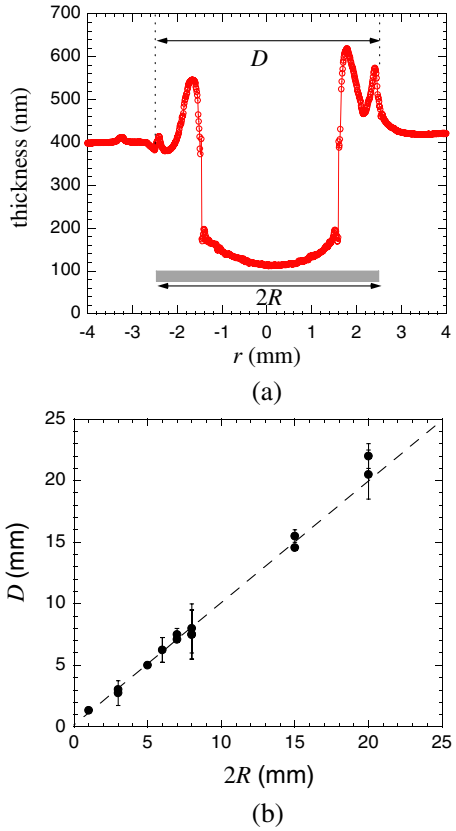

FIG. 2 (color online). (a) An example of a transverse cut in the dip and rim region corresponding to Fig. 1(a) as obtained by optical reflectometry. r is the distance from the center, and the location of the obstacle during evaporation is indicated with a bar. (b) Diameter D of the perturbed film area as a function of the obstacle diameter $2R$.

is an aqueous dispersion of colloidal silica particles (trade name Ludox TMA, particle radius $a = 11$ nm, shear viscosity $\eta = 2$ mPa s). The initial silica volume fraction is 0.1. The film is deposited on the substrate by dip coating, which yields a good control of the initial thickness e_0 (typically 5 μm in our experiments). A plain metal cylinder or a glass fiber (diameter $2R = 1$–15 mm) is located at a short distance ($H \sim 1$ mm) above the volatile film, which impacts the profile of the dried film observed after evaporation [Fig. 2(a)].

We first quantify how an obstacle perturbs evaporation. Evaporation from the surface occurs through diffusive transport of water molecules across the stagnant air layer (of thickness w) adjacent to the film. It can be described by a stationary diffusion equation $\Delta c = 0$, where we denote the vapor concentration by c. The corresponding boundary conditions are a constant concentration c_∞ beyond the boundary layer, a saturation concentration $c_{\rm sat}$ at the liquid surface, and a zero mass flux at the obstacle surface. There is a 50% humidity in the experiment, so that $c_\infty = c_{\rm sat}/2$. The w value can be estimated from the known mass flux J at $r \to \infty$ (far from the obstacle). Instead of the mass flux we operate in what follows with the evaporation speed

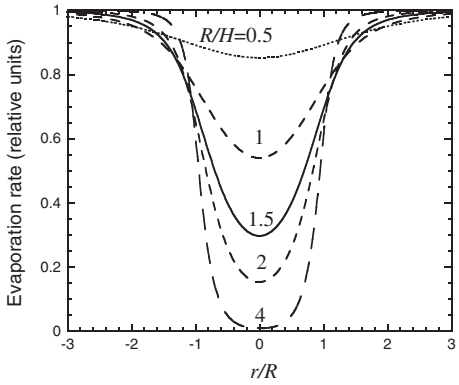

FIG. 3. u/u_∞ as a function of the radial distance below the obstacle. u is obtained numerically from the problem described in the text for $H = 1$ mm, $w = 4.5$ mm, and different values of the ratio $R/H \in (0.5, 4)$.

$u = J/\rho_L$ ($\rho_L$is the liquid density), i.e., the rate of the decrease of the liquid layer thickness. Far from the obstacle it is

$$u_\infty = D_{\rm vap} \frac{c_{\rm sat} - c_\infty}{w}, \qquad (1)$$

where $D_{\rm vap}$ is the vapor diffusivity in the air.

For ambient conditions, u_∞ is about 50 nm/s, and Eq. (1) leads to w of the order of 5 mm. Figure 3 shows the calculated u/u_∞ as a function of the distance r from the center of the obstacle, for aspect ratios R/H between 0.5 and 4. Evaporation is reduced under the obstacle ($r \leq R$), and nearly vanishes for ratios R/H larger than 4. This argument predicts that a liquid ''bump'' should form under the obstacle [Fig. 4(a)]. We confirmed it by measuring the film thickness at two locations, one where evaporation had been obstructed and another one where it had not. An optical fiber connected to a reflectometer was used to measure the film thickness at one location. At the same time, it was used as an obstacle of diameter $2R = 3$ mm. By quickly displacing the optical probe between positions A and B, as sketched in Fig. 4(a), we compared the film thickness below the obstacle and in the rest of the film.

The series with solid squares in Fig. 4(b) shows how the film thickness e decreases under the obstacle, here placed at a height $H = 1$ mm above the liquid surface. In the first regime ($t < 100$ s), the thickness decreases by $u = 25 \pm 5$ nm/s, i.e., with a rate smaller than that observed far from the obstacle where it is $u_\infty = 45 \pm 5$ nm/s, in good agreement [11] with Fig. 3. In the second regime ($t > 100$ s), the film thins much faster. The data shown with open circles are obtained for another film of the same composition and similar initial thickness e_0, but for which the position of the optical fiber was shifted laterally by 4 mm (larger than 3 mm of the fiber diameter) when $t = 75$ s as sketched in Fig. 4(a). This experiment reveals a sharp difference in film thickness between positions A and B, which points out to the existence below the obstacle of a liquid bump, whose height h here is 1500 ± 100 nm.

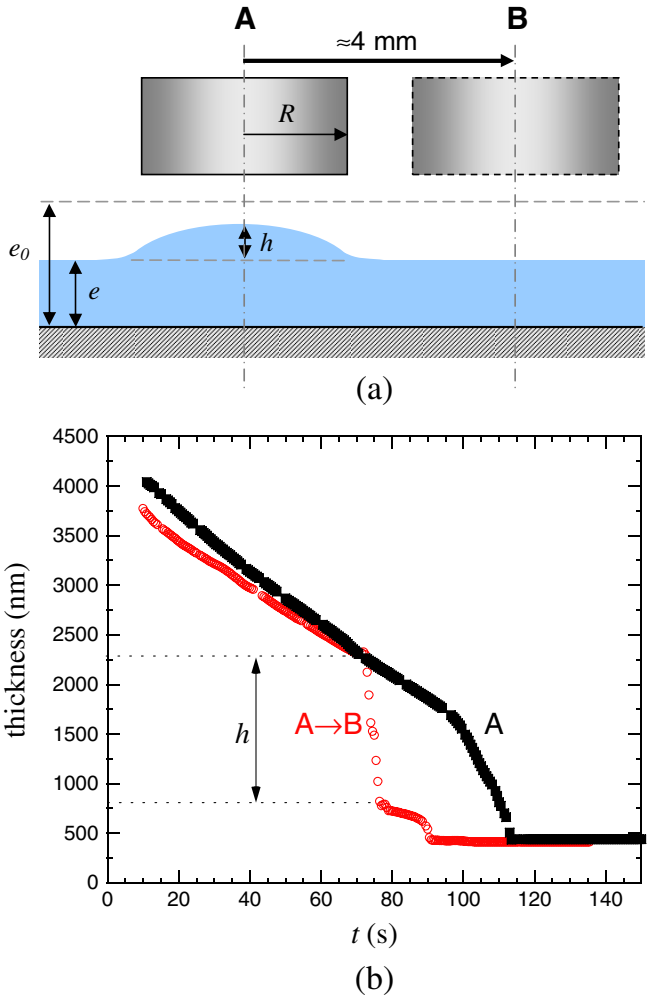

FIG. 4 (color online). (a) By using an optical fiber (of diameter $R = 3$ mm; connected to a reflectometer) as an obstacle, we followed the time evolution of the film thickness below the obstacle (location A). The fiber was also quickly shifted laterally (from A to B) to compare the film heights at these locations. (b) Measurements of film thicknesses during evaporation: (i) the optical fiber is kept at the same location (A), solid squares; the liquid evaporates and the film becomes solid at $t \approx 112$ s. (ii) The optical fiber is displaced from A to B at $t \approx 75$ s (open circles). A sharp decrease in thickness reveals the presence under the obstacle of a liquid "bump" of height $h \approx 1500$ nm.

We performed similar experiments by varying the time t at which the optical fiber is moved, i.e., during the aging of the film. We always observed a bump below the obstacle placed at $H = 1$ mm above the film surface. The bump height h is measured as a function of the lowering of the film $e_0 - e$, where e is the current film thickness. Since the evaporation rate does not vary with time [Fig. 4(b)], $e = e_0 - u_\infty t$ and $e + h = e_0 - ut$ so that $h = (e_0 - e) \times (1 - u/u_\infty)$. The corresponding results are displayed in Fig. 5: the bump gets more and more pronounced as the surrounding film evaporates. If evaporation were negligible below the obstacle, and without any surface tension driven flow, we would see the maximum possible height

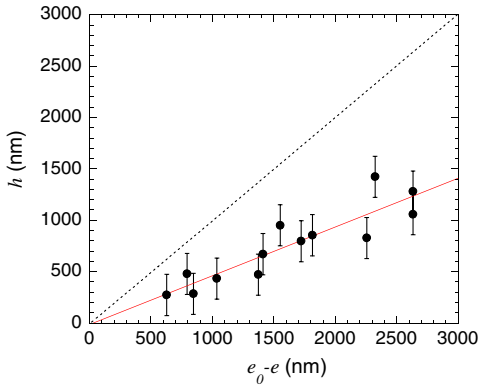

FIG. 5 (color online). Bump height h under the obstacle as a function of the lowering $e_0 - e$ of the surrounding film [see Fig. 4(a)], which is a quantity proportional to the evaporation duration. As the film evaporates, the bump gets higher. Without any evaporation below the obstacle, we would have $h = e_0 - e$ (dotted line); we rather observe $h = (e_0 - e)/2$.

$h = e_0 - e$ (dotted line in the figure). Instead we find $h = (e_0 - e)/2$, in agreement with the theoretical u/u_∞ value [11], as if surface tension did not act to level the film, which we now discuss.

Surface tension γ tends to level any bump or hole at a horizontal liquid surface. We can evaluate the time scale of the leveling, and compare it with the evaporation time. The bump is quite flat (height $h = 1$–2 μm, radius $R = 1$–2 mm), and its curvature scales as h/R^2. This yields a Laplace pressure gradient of the order of $\gamma h/R^3$, a quantity larger than the gravitational force $\rho g h/R$ at the millimeter scale R of the bump. If the flow driven by this pressure gradient has a mean velocity v, the resisting viscous force scales as $\eta v/e^2$. Consequently, the leveling time of the bump is $\tau \sim (\eta/\gamma)(R^4/e^2 h) \sim 10^5$ s, much longer than the time scale of evaporation (about 100 s). In this estimation we neglect the increase of the viscosity due to the increase of the particle concentration, which would yield even larger leveling times.

A bump can thus persist below the obstacle and coexist with the evaporating film. Once the film evaporation is completed beyond the bump, the bump (protected by the obstacle) becomes a drop surrounded by a ring of a wet solidified film (beyond the obstacle), which is itself surrounded by a dry film [Fig. 6]. This geometry induces a strong liquid flow, as revealed by the second regime in Fig. 4(b) (for $t > 100$ s), where the liquid is observed to vanish much quicker than before. This flow can result from a capillary suction by the pores of the solidified film soaked with liquid that evaporates from its surface.

The Laplace pressure difference $\Delta p \sim 10^7$–10^8 Pa is created between the bulk of the drop and the liquid menisci in the nanopores at the surface of the wet solid (of the size 1–10 nm). The liquid evaporation creates a quasistationary outward radial flow [velocity: $v(r)$] which is well described by the following model derived from that of [8]. The film thickness is $d = e(t \to \infty) \approx 500$ nm [Fig. 4(b)] and the

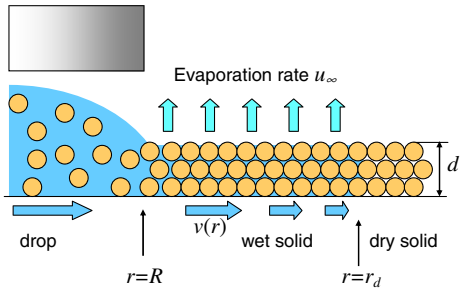

FIG. 6 (color online). When the film surrounding the bump dries, liquid is driven from the bump into a narrow ring of wet solid film, where it evaporates. The flow rate through the pores of the wet solid film balances the evaporative losses at the surface of this wet solid. The flow becomes vanishingly small at the position r_d where the liquid is completely evacuated.

volume fraction ϕ of the solid particles should correspond to the random close packing limit, $\phi = 0.64$. By assuming that the evaporation rate u is constant along the film ($u = u_\infty$), the liquid volume conservation implies the following expression valid for $r \geq R$:

$$d\frac{\partial v}{\partial r} = -u_\infty. \tag{2}$$

Equation (2) results in $v(r) = v(R) - (r - R)u_\infty/d$ and means that the flow stagnates at $r = r_d > R$. One obtains

$$dv(R) = (r_d - R)u_\infty. \tag{3}$$

The r_d value is defined by the pressure drop along the textured film that obeys the Darcy law

$$\frac{\partial p}{\partial r} = -\frac{\mu}{\kappa}v(r), \tag{4}$$

where $\kappa = a^2(1 - \phi)^3/45\phi^2$ is the Carman-Kozeny permeability of the wet solid and $\mu = 1$ mPa s is the water viscosity. By using Eq. (2) and the boundary condition $p(r_d) = p(R) - \Delta p$, one obtains $\Delta p = \mu u_\infty (r_d - R)^2/2d\kappa$, from which r_d can be deduced and then used in Eq. (3) to obtain $v(R)$. The latter quantity serves directly in the calculation of the time $\tau_i = V/2\pi dRv(R)$ needed to empty the drop of the volume $V = \pi hR^2/2$. The substitution of the numerical values results in $\tau_i = 10$ s, which is the time scale visible in Fig. 4(b).

Thus we interpret this fast second regime as resulting from the capillary suction-driven flow. All the conditions required for such a situation are fulfilled: a drop sits on a solid whose texture provides a strong pinning. As a consequence, liquid radially flows inside the drop to supply the contact line region. This flow drives the colloidal particles, which accumulate and form a rim, while the rest of the drop depletes, giving birth to a dip after evaporation similar to coffee stain patterns [1–6]. It is visible in Fig. 2(a) that the rim sets at the periphery of the obstacle. In addition, by integrating the profile, we checked that the material contained in the rim corresponds to the matter transported out of the dip. If the contact line remains immobile during the whole droplet evaporation, a single rim is observed. For weaker pinning, the line may jump onto a new position closer to the droplet center [12], which generates two concentric rims. Such a geometry is sometimes observed in our experiments [Fig. 1(b)].

In summary, we show how obstacles can be used to pattern thin colloidal films. This method is versatile since the obstacles can be manipulated easily, and even possibly removed, thus allowing creation of dips of the same diameter but different depths. It constitutes a simple way to structure the surface of a film of nanometric thickness, to provide desired optical, electrical, or wetting properties. In addition, the formation of the patterns (dips and rims) was shown to involve original effects: (i) A drop forms below the obstacle and coexists transiently with a wet film. (ii) Later, it coexists with dry films, which leads to a strong suction and evaporation of the liquid. This is an original scenario, alternative to the conventional description of the "coffee stain" effect [1]. (iii) Finally, it is interesting to point out that, even at the nanoscopic scale of our films, colloidal material can be transported very efficiently, by using a nonuniform evaporation.

We thank Hervé Willaine for help and guidance with the use of the optical profilometer. This work has been supported by ANR (BLAN-3_144452 "CRUNCH").

[1] R. D. Deegan, O. Bakajin, T. F. Dupont, G. Huber, S. R. Nagel, and T. A. Witten, Nature (London) **389**, 827 (1997).
[2] R. D. Deegan, O. Bakajin, T. F. Dupont, G. Huber, S. R. Nagel, and T. A. Witten, Phys. Rev. E **62**, 756 (2000).
[3] H. Hu and R. Larson, J. Phys. Chem. B **106**, 1334 (2002).
[4] B. J. Fischer, Langmuir **18**, 60 (2002).
[5] Y. O. Popov, Phys. Rev. E **71**, 036313 (2005).
[6] G. Berteloot, C.-T. Pham, A. Daerr, F. Lequeux, and L. Limat, Europhys. Lett. **83**, 14003 (2008).
[7] A. F. Routh and W. B. Russel, AIChE J. **44**, 2088 (1998).
[8] L. Goehring, W. J. Clegg, and A. F. Routh, Langmuir **26**, 9269 (2010).
[9] D. J. Harris, H. Hu, J. C. Conrad, and J. A. Lewis, Phys. Rev. Lett. **98**, 148301 (2007).
[10] D. J. Harris and J. A. Lewis, Langmuir **24**, 3681 (2008).
[11] Note that the calculated u value in Fig. 3 should be averaged over the fiber diameter to be compared with the experiment. This results in the theoretical value $u/u_\infty = 0.43$ for $R/H = 1.5$.
[12] L. Shmuylovich, A. Q. Shen, and H. A. Stone, Langmuir **18**, 3441 (2002).